Rare Met. (2021) 40(3):513–520
https://doi.org/10.1007/s12598-020-01615-x

RARE METALS
www.editorialmanager.com/rmet

ORIGINAL ARTICLE

Enhancing room-temperature thermoelectric performance of n-type Bi_2Te_3-based alloys via sulfur alloying

Feng Liu, Ye-Hao Wu, Qi Zhang, Tie-Jun Zhu*, Xin-Bing Zhao

Received: 15 August 2020 / Revised: 9 September 2020 / Accepted: 10 September 2020 / Published online: 22 October 2020

Abstract Bismuth-telluride-based alloys are the best thermoelectric materials used in commercial solid-state refrigeration near room temperature. Nevertheless, for n-type polycrystalline alloys, their thermoelectric figure of merit (zT) values at room temperature are often less than 1.0, due to the high electron concentration originating from the donor-like effect induced by the mechanical deformation process. Herein, carrier concentration for better performance near room temperature was optimized through manipulating intrinsic point defects by sulfur alloying. Sulfur alloying significantly decreases antisite defects concentration and suppresses donor-like effect, resulting in optimized carrier concentration and reduced electronic thermal conductivity. The hot deformation process was also applied to improve carrier mobility due to the enhanced texture. As a result, a high zT value of 1 at 300 K and peak zT value of 1.1 at 350 K were obtained for the twice hot-deformed $Bi_2Te_{2.7}Se_{0.21}S_{0.09}$ sample, which verifies sulfur alloying is an effective method to improve thermoelectric performance of n-type polycrystalline Bi_2Te_3-based alloys near room temperature.

Keywords Bismuth telluride; Thermoelectric; Point defect; Sulfur alloying; Hot deformation

F. Liu, Y.-H. Wu, Q. Zhang, T.-J. Zhu*, X.-B. Zhao
State Key Laboratory of Silicon Materials, School of Materials Science and Engineering, Zhejiang University, Hangzhou 310027, China
e-mail: zhutj@zju.edu.cn

1 Introduction

Thermoelectric (TE) materials, which can realize direct interconversion between heat and electric energy, have been extensively studied for solid-state refrigeration in past decades [1, 2]. The energy conversion efficiency for TE device is determined by the materials' dimensionless figure of merit $zT = S^2\sigma/\kappa$, where S, σ, κ are the Seebeck coefficient, electrical conductivity, thermal conductivity (including carrier contribution κ_e and phonon contribution κ_L) and absolute temperature, respectively. As S, σ and κ are strongly coupled with carrier concentration n, optimizing n is a foremost procedure to improve TE materials performance [3–5].

For decades, bismuth-telluride-based alloys with layered structure have been the only TE materials realizing widely commercial application [2]. Both n-type and p-type Bi_2Te_3-based quasi-single crystals are prepared by zone melting (ZM), which exhibit maximum zT (zT_{max}) of ~ 1.0 near room temperature [6, 7]. Nevertheless, owing to the van der Waals bonding, their easy-cleavage nature increases the expenditure for device fabrication and weakens reliability. To improve the mechanical properties, polycrystalline Bi_2Te_3-based alloys have been prepared by powder metallurgical methods, such as mechanical alloying (MA), ball milling (BM), melt spinning or solvothermal synthesis followed by hot pressing (HP) or spark plasma sintering (SPS) [8–12]. For p-type polycrystalline $(Bi, Sb)_2Te_3$ alloys, $zT_{max} > 1.2$ can be easily attained at 300-350 K, benefiting from substantially reduced thermal conductivity [13–15].

However, for n-type polycrystalline $Bi_2(Te, Se)_3$ alloys, their zT_{max} often appears at elevated temperature and less than 1.0, which hinders their further commercial

application [16, 17]. On the one hand, the layered-structure nature of Bi_2Te_3 alloys renders the anisotropy of TE performance, which is stronger in n-type [18–20]. The random arrangement of grains destroys the (00l) texture leading to deteriorated zT values [21]. Hot deformation (HD) process can significantly enhance texture and improve zT values [22–24]. Apart from that, the extreme high electron concentration deviated from optimum value also leads to the deteriorated zT near room temperature [25].

The single crystals grown from stoichiometric bismuth telluride always show an excess of cation and excess Bi atoms can occupy Te sites to form negative charged antisite defects Bi'_{Te}, which explains the p-type conduction behavior [26, 27]. For polycrystalline Bi_2Te_3-based alloys, the pulverization process of ingots by mechanical grinding induces the non-basal slip, in which the cation vacancies and anion vacancies with 2:3 ratio are generated [28]. Navrátil et al. [29] proposed a donor-like effect which increases the electron concentration due to the interaction between vacancies and antisite defects as below:

$$2V'''_{Bi} + 3V^{\cdot\cdot}_{Te} + Bi'_{Te} \rightarrow 2Bi^{\times}_{Bi} + 4V^{\cdot\cdot}_{Te} + 6e \quad (1)$$

where V'''_{Bi} and $V^{\cdot\cdot}_{Te}$ represent vacancy of Bi and Te, respectively. This formula is also valid for V'''_{Sb}, Sb'_{Te} (Sb_2Te_3) and $V^{\cdot\cdot}_{Se}$, Bi'_{Se} (Bi_2Se_3). One approach to alleviate this effect is utilizing p-type dopants to compensate excessive electrons. Ag, Cu, Pb are widely used p-type dopants [30, 31]. In n-type polycrystalline $Ag_xBi_{2-x}(Te,Se)_3$ alloys, doped Ag atoms form the substitutional defects Ag''_{Bi} and decrease electron concentration [32–34]. But Ag and Cu can rapidly migrate along (001) plane under working electric current, and Pb is poisonous [35].

Manipulating intrinsic point defects is also effective in tuning the carrier concentration of Bi_2Te_3-based materials [36]. Zhu et al. [37] summarized a (χ−r) model, in which the formation of vacancies and antisite defects is influenced by the differences of electronegativity χ and the covalent radius r. Sulfur alloying can be applied to reduce formation energy of anion vacancies and promote electron generation [38]. Horak et al. [39] decreased the hole concentration by increasing the sulfur content in $Bi_2Te_{3-x}S_x$ single crystals and achieved p–n transition at $x = 0.15$. Liu et al. [40] combined MA and SPS methods to fabricate $Bi_2Te_{2.7-x}Se_{0.3}S_x$ bulks and increased electron concentration with increasing sulfur content. However, little work adopted sulfur alloying to regulate the donor-like effect, despite much work was focused on the Se alloying [41, 42]. But excessive Se alloying deteriorates zT values near room temperature, originating from the enlarged band gap E_g and the strengthened alloy scattering on carriers [42, 43]. Owing to the smaller covalent radius and larger electronegativity of sulfur, using a lower content of sulfur as alloying element can effectively prevent the generation of antisite defects and suppress the donor-like effect, which is beneficial for maintaining high power factor.

Herein, a combination of sulfur alloying and HD process is reported. Sulfur alloying successfully suppresses the donor-like effect, and HD process enhances the texture. The optimized carrier concentration and the enhanced carrier mobility together lead to a boosted zT value near room temperature. For further enhancement, twice HD process was applied to the $Bi_2Te_{2.7}Se_{0.21}S_{0.09}$ sample. As a result, a high zT value of 1.0 at 300 K and peak zT value of 1.1 at 350 K are obtained. This work verifies the feasibility of sulfur alloying to regulate the donor-like effect and improves the room temperature TE performance of n-type polycrystalline Bi_2Te_3-based alloys.

2 Experimental

Highly pure element chunks (5 N, Emei Semiconductor Materials Research Institute) of Se, Te, Bi and sulfur powder (5 N, Alfa Aesar) were weighted according to the stoichiometric $Bi_2Te_{2.79-x}Se_{0.21}S_x$ ($x = 0$, 0.05, 0.07, 0.09, 0.12, 0.18 and 0.25) and sealed into quartz tubes at 1×10^{-3} Pa. The mixtures were melted in the Muffle furnace at 1073 K for 10 h and rocked every two hours to ensure composition homogeneity before cooled in furnace. The obtained ingots were ball-milled (MM200, Retzsch) into fine powders at 20 Hz for 20 min. Subsequently, the powders were loaded into Φ12.7 mm graphite dies and hot-pressed at 773 K for 30 min with 80 MPa uniaxial pressure (4505 J, MRF). Then, the obtained cylinder was hot-deformed in a larger Φ20 mm graphite die at 823 K for 30 min with 80 MPa uniaxial pressure. Final samples were named as HD-Sx. For the HD-S0.05 and HD-S0.09 samples, a disk of 12.7 mm in diameter was cut and hot-deformed again in the same condition, named as HD2-S0.05 and HD2-S0.09.

The phase structures of all powders were investigated by X-ray diffraction (XRD) on a Rigaku D/MAX-2550P diffractometer with Cu Kα radiation. The chemical compositions were checked by the electron probe micro-analyzer (EPMA, JEOL JXA-8100) using a wavelength dispersive spectroscope. The electrical conductivity (σ) and Seebeck coefficient (S) were simultaneously measured on a commercial Linseis LSR-3 system. The thermal conductivity (κ) was calculated using $\kappa = \rho D C_p$, where ρ is the density of sample determined by Archimedes method, C_p is the specific heat estimated by Dulong–Petit law, and D is the thermal diffusivity measured on a Netzsch LFA 467 instrument. The samples for in-plane κ measurement were prepared using the method reported by Xie et al. [44]. The estimated measurement uncertainties are 3% for electrical

conductivity, 5% for the Seebeck coefficient and 5% for thermal diffusivity. The Hall coefficient (R_H) at 300 K was collected on a Mini Cryogen Free Measurement System (Cryogenic Limited, UK) with magnetic field varied between ± 4.0 T. Then, the Hall carrier concentration (n_H) and Hall mobility (μ_H) were determined via $n_H = 1/eR_H$ (e is the electron charge) and $\mu_H = \sigma R_H$, respectively. To be noted, all properties were measured along the direction perpendicular to the pressure.

3 Results and discussion

The powder XRD patterns in Fig. 1a show that all samples have a pure rhombohedral $R\bar{3}m$ phase and no secondary phases are observed. As shown in Fig. 1b, the lattice parameters of $Bi_2Te_{2.79-x}Se_{0.21}S_x$ decrease with increasing nominal content of sulfur, resulting from the smaller covalent radius of sulfur (0.104 nm) than Te (0.137 nm). The variation of lattice parameters indicates that sulfur has been successfully doped into the matrix of $Bi_2Te_{2.79}Se_{0.21}$ and occupies Te sub-lattice sites, which can be further proved by composition characterization. From EPMA measurement results in Table 1, the actual content of sulfur in HD samples increases with increasing nominal content, which is consistent with lattice parameter shrink. The contents of Se and sulfur are lower than their nominal contents. Because of their low boiling point (958 and 718 K, respectively) and high vapor pressure, they inevitably suffer loss during smelting and HD process.

Figure 2 displays the Hall concentration n_H and mobility μ_H of all HD-Sx samples at room temperature. It can be seen that the n_H decreases with x increasing, due to the weakened donor-like effect. The formation energy of antisite defects is dependent on the difference of electronegativity and the covalent radius. Enlarging the differences can prevent the generation of antisite defects [37]. From Table 2, the differences in covalent radius and electronegativity between Bi-sulfur are larger than Bi-Te or Bi-Se, which increase the formation energy of antisite defects and in turn decrease their concentrations. From Eq. (1), the concentration of anion vacancy induced by the donor-like effect is simultaneously decreased. Thus, as x varies from 0 to 0.12, the n_H decreases from 8.5×10^{19} cm^{-3} to 1.9×10^{19} cm^{-3}.

Table 1 Chemical compositions detected by EPMA for HD-Sx samples

Nominal composition	EPMA composition
$Bi_2Te_{2.79}Se_{0.21}$	$Bi_2Te_{2.782}Se_{0.185}$
$Bi_2Te_{2.74}Se_{0.21}S_{0.05}$	$Bi_2Te_{2.743}Se_{0.186}S_{0.029}$
$Bi_2Te_{2.72}Se_{0.21}S_{0.07}$	$Bi_2Te_{2.717}Se_{0.189}S_{0.055}$
$Bi_2Te_{2.7}Se_{0.21}S_{0.09}$	$Bi_2Te_{2.696}Se_{0.191}S_{0.072}$
$Bi_2Te_{2.67}Se_{0.21}S_{0.12}$	$Bi_2Te_{2.675}Se_{0.191}S_{0.103}$
$Bi_2Te_{2.61}Se_{0.21}S_{0.18}$	$Bi_2Te_{2.609}Se_{0.187}S_{0.156}$
$Bi_2Te_{2.54}Se_{0.21}S_{0.25}$	$Bi_2Te_{2.563}Se_{0.179}S_{0.218}$

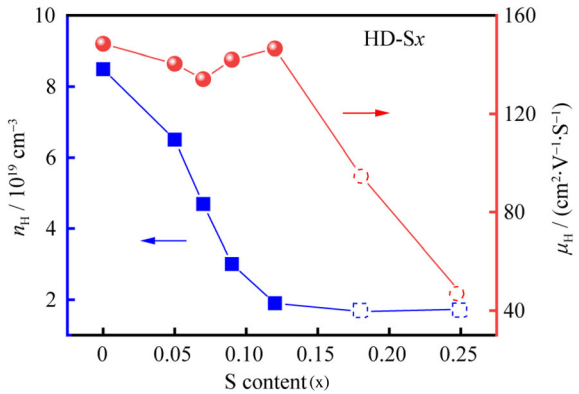

Fig. 2 Room temperature carrier concentration and mobility as a function of sulfur content x in HD-Sx samples, where empty dots meaning that measured parameters may be not correct due to severely intrinsic conduction

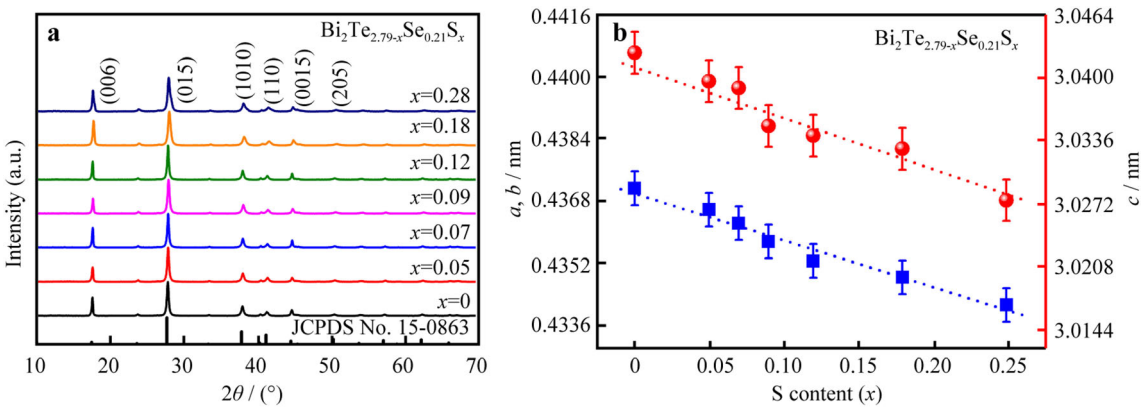

Fig. 1 **a** Powder XRD patterns of $Bi_2Te_{2.79-x}Se_{0.21}S_x$; **b** lattice parameters as a function of sulfur content x for $Bi_2Te_{2.79-x}Se_{0.21}S_x$

Table 2 Covalent radius and electronegativity of Bi, Te, Se and sulfur [37]

Element	Covalent radius/nm	Electronegativity
Bi	0.150	1.90
Te	0.137	2.10
Se	0.118	2.55
Sulfur	0.104	2.58

The fluctuation of μ_H is more complicated. On the one hand, sulfur alloying will introduce additional alloy scattering and decrease the μ_H. On the other hand, the lower n_H and reduced intrinsic point defects will weaken the carrier scattering, which increases the μ_H. Finally, the μ_H first decreases and then increases with increasing x. For narrow band gap semiconductors, the electrons in the valance band can be thermally excited into the conduction band, leaving a hole in the valance band. Consequently, with increasing temperature, the more electron–hole pairs are generated and the measured n_H increases. The phenomenon is more significant when the E_g is small or the majority carrier concentration is relatively low [45]. Hence, for Samples HD-S0.18 and HD-S0.25, they are severely intrinsically excited at room temperature. Considering their measured Hall data contains the contribution from thermal excitation and are not accurate anymore, hollow points are used to distinguish.

An enhancement in the Seebeck coefficient S near room temperature was obtained due to the decreased n_H, as shown in Fig. 3a. Here, a single parabolic band (SPB) model [46] limited by acoustic phonon scattering is used to describe the correlation between S and n_H. In this model, S and n_H are defined by using following equations:

$$S = \frac{k}{e}\left(\frac{2F_1(\eta)}{F_0(\eta)} - \eta\right) \tag{2}$$

$$n_H = \frac{8\pi}{3}\left(\frac{2m^* kT}{h^2}\right)^{3/2} \frac{2F_0^2(\eta)}{F_{-1/2}(\eta)} \tag{3}$$

where e is the electron charge, k is the Boltzmann constant, h is the Planck constant, m^* is density-of-state effective mass, η is the reduced Fermi level. And $F_j(\eta)$ is Fermi integral defined by:

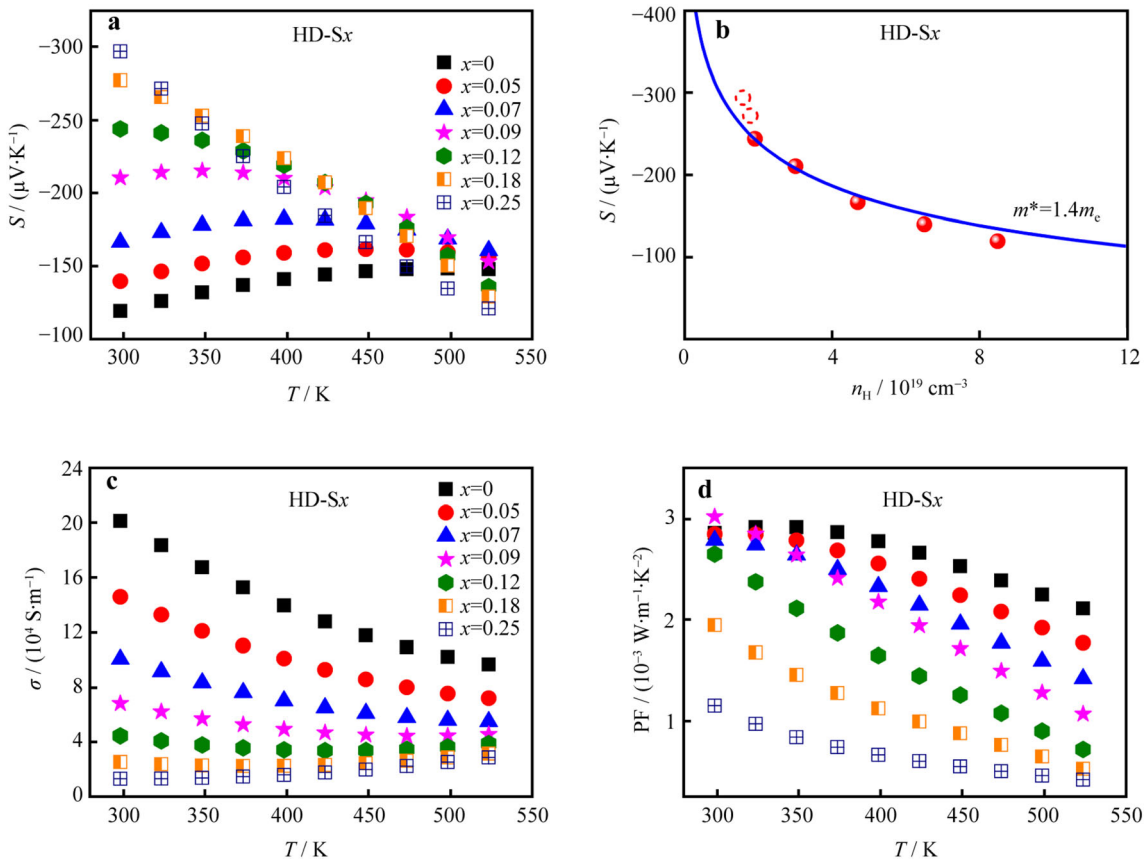

Fig. 3 Temperature dependences of **a** Seebeck coefficient, **c** electrical conductivity, **d** PF in HD-Sx samples; **b** room temperature Pisarenko plot of HD-Sx samples

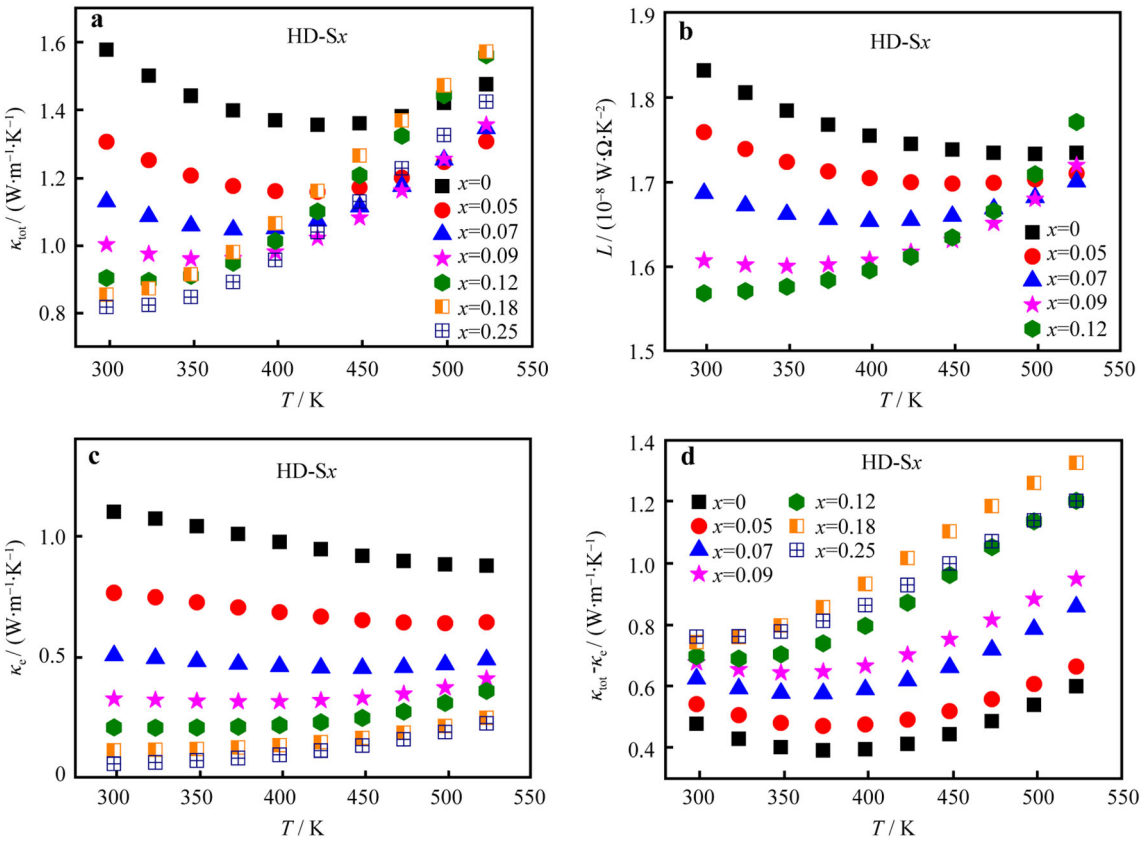

Fig. 4 Temperature dependences of **a** total thermal conductivity, **b** Lorentz number, **c** electronic thermal conductivity and **d** lattice thermal conductivity in HD-Sx samples

$$F_j(\eta) = \int_0^\infty f\varepsilon^j \mathrm{d}\varepsilon = \int_0^\infty \frac{\varepsilon^j \mathrm{d}\varepsilon}{1+\exp[\varepsilon-\eta]} \tag{4}$$

From Fig. 3b, the S increases with decreasing n_H, which is accordant with experiment results in Figs. 2 and 3a. And no obvious differences in m^* between different HD-Sx samples can be seen (m_e is the mass of the electron), which indicates negligible influence on band structure by sulfur alloying. Furthermore, the corresponding temperature (named as T_{max}) of maximum S (named as S_{max}) is downshifting with rising sulfur content, which is beneficial for better electrical properties near room temperature. The downshift of T_{max} can be explained in two aspects: one is the decreased E_g and the other is the reduced majority carrier concentration [47]. Herein, the E_g is roughly evaluated according to $E_g = 2eS_{max}T_{max}$ [46] and its values maintain at 0.14-0.15 eV. Hence, the reduced carrier concentration with increasing x is the reason for the downshift of T_{max}. The electrical conductivity σ was calculated using $\sigma = ne\mu$. As shown in Fig. 3c, for all samples, the σ exhibits typical degenerate semiconductor conduction behavior, where σ decreases with increasing temperature. Owing to the slight influence on μ_H for sulfur alloying, the σ is mainly determined by n_H. The σ near room temperature is deteriorated due to sulfur alloying induced decrease in n_H.

Figure 3d plots the temperature dependence of power factor (PF). The PF was calculated using PF = $S^2\sigma$. When $x \leq 0.12$, sulfur alloying reduces the extremely high n_H and enhances S. But it simultaneously deteriorates μ_H and decreases σ. Combined the two opposite factors, the room temperature PF remains unchanged as the sulfur content increases. When $x > 0.12$, the severely intrinsic conduction causes a rapid drop in room temperature PF.

Figure 4 presents the effect of sulfur alloying on thermal conductivity. The specific heat and density of HD-Sx samples are shown in Table 3. Owing to the notable drop in σ, the total thermal conductivity (κ_{tot}) of HD-Sx sample at room temperature monotonically decreases from 1.58 to 0.82 W·m^{-1}·K^{-1}, as shown in Fig. 4a. The electronic thermal conductivity (κ_e) was estimated according to $\kappa_e = L\sigma T$, and L is the Lorenz number defined by SPB model as below [46]:

$$L = \frac{k^2}{e^2}\frac{3F_0F_2 - 4F_1^2}{F_0^2} \tag{5}$$

The calculated L and κ_e are plotted in Fig. 4b, c. For Samples HD-S0.18 and HD-S0.25, they are severely

Table 3 Specific heat and density of HD-Sx samples

Sample	Specific heat/(J·g^{-1}·K^{-1})	Density/(g·cm^{-3})
HD-S0	0.1577	7.225
HD-S0.05	0.1587	7.464
HD-S0.07	0.1591	7.473
HD-S0.09	0.1595	7.410
HD-S0.12	0.1601	7.431
HD-S0.18	0.1612	7.442
HD-S0.25	0.1626	7.421

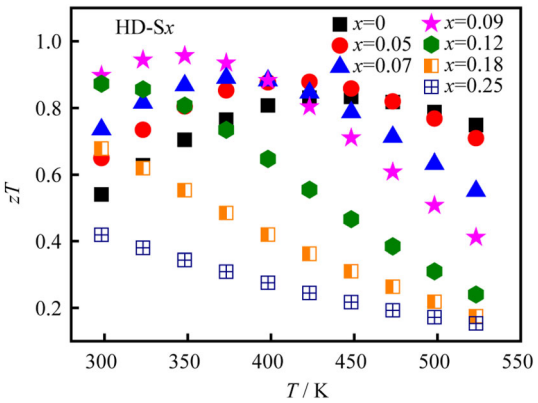

Fig. 5 Temperature dependences of zT in HD-Sx samples

intrinsically excited at room temperature and regarded as non-degenerate semiconductor. Consequently, their L values were chosen as 1.5×10^{-8} W·Ω·K^{-2}. The κ_e near room temperature monotonically decreases with x increasing, which is in accordance with the decrease of σ.

Then, the lattice thermal conductivity (κ_L) was obtained by subtracting κ_e from κ_{tot}. It should be noticed that here the κ_L contains the bipolar thermal conductivity (κ_b), originating from intrinsic excitation. Figure 4d shows the temperature dependence of κ_L. The κ_L increases in the whole temperature range by sulfur alloying. Normally, sulfur alloying should introduce stronger mass and strain fluctuations, which decrease the κ_L [40]. However, in this work, sulfur alloying significantly suppresses donor-like effect and induces the rapid drop on n_H. Hence, the bipolar effect becomes more remarkable, resulting in the increase of κ_L [48]. Notably, the decrease of κ_e is dominant and PF maintains at relative high values with increasing x, which is beneficial for better zT values near room temperature.

Figure 5 displays the temperature dependence of zT in the HD-Sx samples. Owing to the high $n_H \sim 8.5 \times 10^{19}$ cm^{-3} of HD-S0 sample, it exhibits a low zT value of 0.54 at room temperature. With increasing x, n_H continuously decreases and room temperature zT value is enhanced. Finally, a highest zT value of 0.9 at 300 K is obtained in the HD-S0.09 sample, with an optimized n_H of 3×10^{19} cm^{-3}. Further increasing x, the bipolar

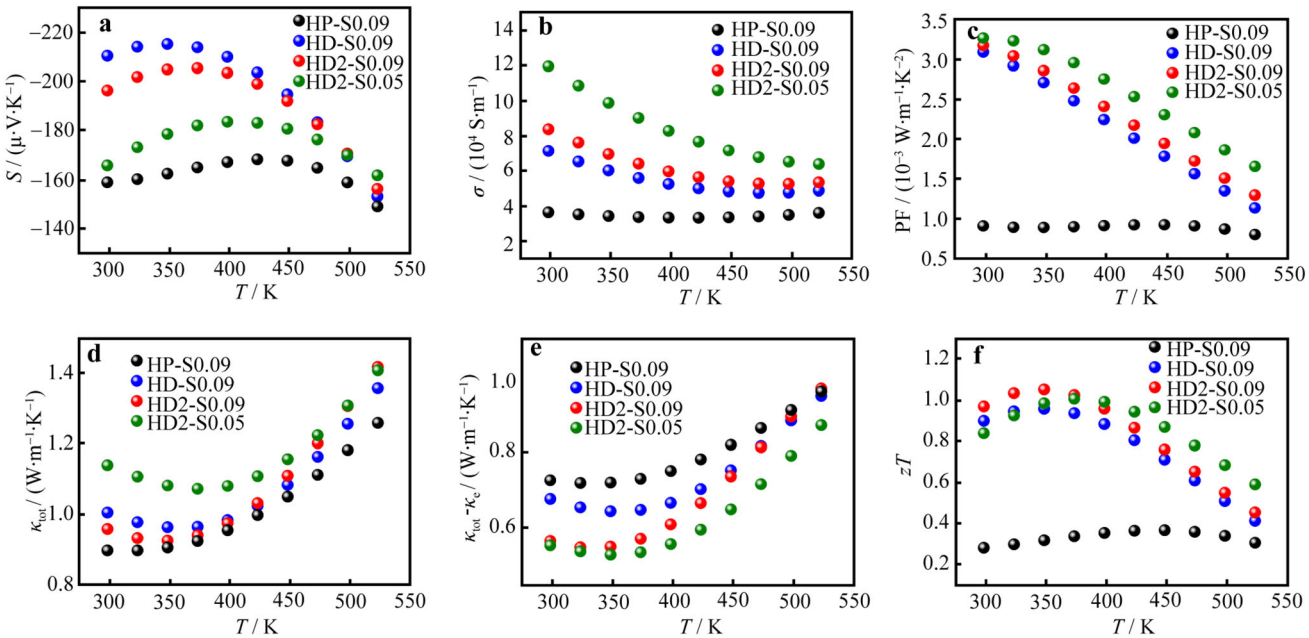

Fig. 6 Temperature dependences of **a** Seebeck coefficient, **b** electrical conductivity, **c** power factor, **d** total thermal conductivity, **e** lattice thermal conductivity and **f** zT in HP-S0.09, HD-S0.09, HD2-S0.09 and HD2-S0.05 samples

conduction gradually becomes more significant and zT value deteriorates instead.

According to our previous work, the zT value of n-type $Bi_2(Te,Se)_3$ alloys could be further enhanced by repetitive hot deformation, which can be attributed to the enhancement of texture [49, 50]. Therefore, one more hot-deformation process on the HD-S0.05 and HD-S0.09 samples was applied. Their TE properties are shown in Fig. 6, where the results of hot-pressed $Bi_2Te_{2.7}Se_{0.21}S_{0.09}$ sample (HP-S0.09) are also plotted. For the $Bi_2Te_{2.7}Se_{0.21}S_{0.09}$ sample, hot deformation process significantly enhances the σ originating from the increased μ_H induced by the enhanced in-plane texture. The κ_L substantially decreases, originating from the multi-scale defects generated by the deformation process [51]. Hence, the zT value at room temperature improves from 0.3 to 1.0 via twice hot deformation. For the HD2-S0.05 sample, the decreased S and enhanced σ comparing to that of the HD2-S0.09, which are ascribed to the increased electron concentration, resulting in the same PF values. In spite of their same κ_L values, the κ_{tot} of HD2-S0.05 sample is higher, originating from the higher σ. Finally, a highest zT value of 1.0 at 300 K for HD2-S0.09 is obtained, which is favorable for high efficiency refrigeration in the vicinity of room temperature.

4 Conclusion

In this work, the TE performance of n-type polycrystalline $Bi_2(Te,Se)_3$ alloys at room temperature by sulfur alloying was successfully optimized. Owing to the larger discrepancy on covalent radius and electronegativity for Bi-sulfur compared to Bi-Te and Bi-Se, sulfur alloying significantly reduces the concentration of antisite defects, suppresses the donor-like effect and in turn causes the rapid drop in n_H, which is beneficial for higher Seebeck coefficient and lower electronic thermal conductivity at room temperature. As a result, a high zT value of 1.0 at 300 K and peak zT value of 1.1 at 350 K are obtained for HD2-S0.09 sample, which is promising for practical use in solid-state refrigeration in the vicinity of room temperature.

Acknowledgments This work was financially supported by the National Key Research and Development Program of China (No. 2019YFA0704902) and the National Natural Science Foundation of China (Nos. 51871199 and 61534001).

References

[1] He J, Tritt TM. Advances in thermoelectric materials research: looking back and moving forward. Science. 2017;357(6358):1369.
[2] Heremans JP, Cava RJ, Samarth N. Tetradymites as thermoelectrics and topological insulators. Nat Rev Mater. 2017;2(10):17049.
[3] Zhu T, Liu Y, Fu C, Heremans JP, Snyder JG, Zhao X. Compromise and synergy in high-efficiency thermoelectric materials. Adv Mater. 2017;29(14):1605884.
[4] Snyder GJ, Toberer ES. Complex thermoelectric materials. Nat Mater. 2008;7(2):105.
[5] Fu T, Xin J, Zhu T, Shen J, Fang T, Zhao X. Approaching the minimum lattice thermal conductivity of p-type SnTe thermoelectric materials by Sb and Mg alloying. Sci Bull. 2019;64(14):1024.
[6] Rowe DM. CRC Handbook of Thermoelectrics. Boca Raton: CRC Press; 1995. 252.
[7] Zhai R, Wu Y, Zhu T, Zhao X. Thermoelectric performance of p-type zone-melted Se-doped $Bi_{0.5}Sb_{1.5}Te_3$ alloys. Rare Met. 2018;37(4):308.
[8] Poudel B, Hao Q, Ma Y, Lan Y, Minnich A, Yu B, Yan X, Wang D, Muto A, Vashaee D, Chen X, Liu J, Dresselhaus MS, Chen G, Ren Z. High-thermoelectric performance of nanostructured bismuth antimony telluride bulk alloys. Science. 2008;320(5876):634.
[9] Zhao X, Ji X, Zhang Y, Zhu T, Tu J, Zhang X. Bismuth telluride nanotubes and the effects on the thermoelectric properties of nanotube-containing nanocomposites. Appl Phys Lett. 2005;86(6):062111.
[10] Li J, Tan Q, Li J, Liu D, Li F, Li Z, Zou M, Wang K. BiSbTe-based nanocomposites with high zT: the effect of SiC nanodispersion on thermoelectric properties. Adv Funct Mater. 2013;23(35):4317.
[11] Tang X, Xie W, Li H, Zhao W, Zhang Q, Niino M. Preparation and thermoelectric transport properties of high-performance p-type Bi_2Te_3 with layered nanostructure. Appl Phys Lett. 2007;90(1):012102.
[12] Li J, Pan Y, Wu C, Sun F, Wei T. Processing of advanced thermoelectric materials. Sci China Technol Sci. 2017;60(9):1347.
[13] Shen J, Zhu T, Zhao X, Zhang S, Yang S, Yin Z. Recrystallization induced in situ nanostructures in bulk bismuth antimony tellurides: a simple top down route and improved thermoelectric properties. Energy Environ Sci. 2010;3(10):1519.
[14] Kim SI, Lee KH, Mun HA, Kim HS, Hwang SW, Roh JW, Yang DJ, Shin WH, Li X, Lee YH, Snyder GJ, Kim SW. Dense dislocation arrays embedded in grain boundaries for high-performance bulk thermoelectrics. Science. 2015;348(6230):109.
[15] Xie W, He J, Kang H, Tang X, Zhu S, Laver M, Wang S, Copley JR, Brown CM, Zhang Q, Tritt TM. Identifying the specific nanostructures responsible for the high thermoelectric performance of $(Bi, Sb)_2Te_3$ nanocomposites. Nano Lett. 2010;10(9):3283.
[16] Liu W, Jie Q, Kim HS, Ren Z. Current progress and future challenges in thermoelectric power generation: from materials to devices. Acta Mater. 2015;87(1):357.
[17] Zhang Q, Fang T, Liu F, Li A, Wu Y, Zhu T, Zhao X. Tuning optimum temperature range of Bi_2Te_3-based thermoelectric materials by defect engineering. Chem Asian J. 2020;15(18):2775.
[18] Delves RT, Bowley AE, Hazelden DW, Goldsmid HJ. Anisotropy of the electrical conductivity in bismuth telluride. Proc Phys Soc. 1961;78(5):838.
[19] Shen J, Hu L, Zhu T, Zhao X. The texture related anisotropy of thermoelectric properties in bismuth telluride based polycrystalline alloys. Appl Phys Lett. 2011;99(12):124102.
[20] Fang T, Li F, Wu Y, Zhang Q, Zhao X, Zhu T. Anisotropic thermoelectric properties of n-type Te-free $(Bi, Sb)_2Se_3$ with

orthorhombic structure. ACS Appl Energy Mater. 2020;3(3):2070.
[21] Yan X, Poudel B, Ma Y, Liu W, Joshi G, Wang H, Lan Y, Wang D, Chen G, Ren Z. Experimental studies on anisotropic thermoelectric properties and structures of n-type $Bi_2Te_{2.7}Se_{0.3}$. Nano Lett. 2010;10(9):3373.
[22] Hu L, Zhang Y, Wu H, Liu Y, Li J, He J, Ao WQ, Liu F, Pennycook SJ, Zeng X. Synergistic compositional-mechanical-thermal effects leading to a record high zT in n-type V_2VI_3 alloys through progressive hot deformation. Adv Funct Mater. 2018;28(35):1803617.
[23] Hu L, Zhu T, Wang Y, Xie H, Xu Z, Zhao X. Shifting up the optimum figure of merit of p-type bismuth telluride-based thermoelectric materials for power generation by suppressing intrinsic conduction. NPG Asia Mater. 2014;6(2):e88.
[24] Pan Y, Li J. Thermoelectric performance enhancement in n-type $Bi_2(TeSe)_3$ alloys owing to nanoscale inhomogeneity combined with a spark plasma-textured microstructure. NPG Asia Mater. 2016;8(6):e275.
[25] Zhao Y, Dyck JS, Hernandez BM, Burda C. Improving thermoelectric properties of chemically synthesized Bi_2Te_3-based nanocrystals by annealing. J Phys Chem C. 2010;114(26):11607.
[26] Miller GR, Li C. Evidence for the existence of antistructure defects in bismuth telluride by density measurements. J Phys Chem Solids. 1965;26(1):173.
[27] Brebrick RF. Homogeneity ranges and Te_2-pressure along the three-phase curves for Bi_2Te_3 and 55–58 at.% Te, peritectic phase. J Phys Chem Solids. 1969;30(3):719.
[28] Schultz JM, McHugh JP, Tiller WA. Effects of heavy deformation and annealing on the electrical properties of Bi_2Te_3. J Appl Phys. 1962;33(8):2443.
[29] Navrátil J, Starý Z, PlecháčEk T. Thermoelectric properties of p-type antimony bismuth telluride alloys prepared by cold pressing. Mater Res Bull. 1996;31(12):1559.
[30] Hao F, Qiu P, Tang Y, Bai S, Xing T, Chu H, Zhang Q, Lu P, Zhang T, Ren D, Chen J, Shi X, Chen L. High efficiency Bi_2Te_3-based materials and devices for thermoelectric power generation between 100 and 300 °C. Energy Environ Sci. 2016;9(10):3120.
[31] Wei Z, Wang C, Zhang J, Yang J, Li Z, Zhang Q, Luo P, Zhang W, Liu E, Luo J. Precise regulation of carrier concentration in thermoelectric BiSbTe alloys via magnetic doping. ACS Appl Mater Interfaces. 2020;12(18):20653.
[32] Zhang X, Ma X, Lu Q, Zhang F, Liu Y, Zhang J, Wang L. Thermoelectric properties of Ag-doped n-type $(Bi_{2-x}Ag_xTe_3)_{0.96} - (Bi_2Se_3)_{0.04}$ pseudobinary alloys. J Electron Mater. 2011;40(5):773.
[33] Wu Y, Zhai R, Zhu T, Zhao X. Enhancing room temperature thermoelectric performance of n-type polycrystalline bismuth-telluride-based alloys via Ag doping and hot deformation. Mater Today Phys. 2017;2(1):62.
[34] Li B, Zhai R, Fang T, Xia K, Wu Y, Zhu T. Mid-temperature thermoelectric performance of zone-melted $Sb_2(Te, Se)_3$ alloys near phase transition boundary. J Materiomics. 2019;5(4):590.
[35] Carlson RO. Anisotropic diffusion of copper into bismuth telluride. J Phys Chem Solids. 1960;13(1):65.
[36] Zhang Q, Gu B, Wu Y, Zhu T, Fang T, Yang Y, Liu J, Ye B, Zhao X. Evolution of the intrinsic point defects in bismuth telluride based thermoelectric materials. ACS Appl Mater Interfaces. 2019;11(44):41424.
[37] Zhu T, Hu L, Zhao X, He J. New insights into intrinsic point defects in V_2VI_3 thermoelectric materials. Adv Sci. 2016;3(7):1600004.
[38] Birkholz VU. Untersuchung der intermetallischen Verbindung Bi_2Te_3 sowie der festen Lösungen $Bi_{2-x}Sb_xTe_3$ und $Bi_2Te_{3-x}Se_x$ hinsichtlich ihrer Eignung als Material für Halbleiter-Thermoelemente. Phys Phys Chem. 1958;13(1):780.
[39] Horak J, Lostak P, Koudelka L, Novotny R. Inversion of conductivity type in $Bi_2Te_{3-x}S_x$ crystals. Solid State Commun. 1985;55(22):1031.
[40] Liu W, Lukas KC, McEnaney K, Lee S, Zhang Q, Opeil CP, Chen G, Ren Z. Studies on the Bi_2Te_3–Bi_2Se_3–Bi_2S_3 system for mid-temperature thermoelectric energy conversion. Energy Environ Sci. 2013;6(2):552.
[41] Hu L, Zhu T, Liu X, Zhao X. Point defect engineering of high-performance bismuth-telluride-based thermoelectric materials. Adv Funct Mater. 2014;24(33):5211.
[42] Pan Y, Wei T, Wu C, Li J. Electrical and thermal transport properties of spark plasma sintered n-type $Bi_2Te_{3-x}Se_x$ alloys: the combined effect of point defect and Se content. J Mater Chem C. 2015;3(40):10583.
[43] Miller GR, Li C, Spencer CW. Properties of Bi_2Te_3–Bi_2Se_3 alloys. J Appl Phys. 1963;34(5):1398.
[44] Xie W, He J, Zhu S, Holgate T, Wang S, Tang X, Zhang Q, Tritt TM. Investigation of the sintering pressure and thermal conductivity anisotropy of melt-spun spark-plasma-sintered $(Bi, Sb)_2Te_3$ thermoelectric materials. J Mater Res. 2011;26(15):1791.
[45] Wang S, Yang J, Toll T, Yang J, Zhang W, Tang X. Conductivity-limiting bipolar thermal conductivity in semiconductors. Sci Rep. 2015;5(1):10136.
[46] May A, Snyder G. Introduction to modeling thermoelectric transport at high temperatures. In: Rowe DM, editor. Materials, Preparation, and Characterization in Thermoelectrics. Boca Raton: CRC Press; 2012. 1.
[47] Li F, Zhai R, Wu Y, Xu Z, Zhao X, Zhu T. Enhanced thermoelectric performance of n-type bismuth-telluride-based alloys via In alloying and hot deformation for mid-temperature power generation. J Materiomics. 2018;4(3):208.
[48] Qin H, Liu Y, Zhang Z, Wang Y, Cao J, Cai W, Zhang Q, Sui J. Improved thermoelectric performance of p-type $Bi_{0.5}Sb_{1.5}Te_3$ through Mn doping at elevated temperature. Mater Today Phys. 2018;6(1):31.
[49] Tang Z, Hu L, Zhu T, Liu X, Zhao X. High performance n-type bismuth telluride based alloys for mid-temperature power generation. J Mater Chem C. 2015;3(40):10597.
[50] Hu L, Gao H, Liu X, Xie H, Shen J, Zhu T, Zhao X. Enhancement in thermoelectric performance of bismuth telluride based alloys by multi-scale microstructural effects. J Mater Chem. 2012;22(32):16484.
[51] Hu L, Wu H, Zhu T, Fu C, He J, Ying P, Zhao X. Tuning multiscale microstructures to enhance thermoelectric performance of n-type bismuth-telluride-based solid solutions. Adv Energy Mater. 2015;5(17):1500411.